



Deposited via The University of Sheffield.

White Rose Research Online URL for this paper:

<https://eprints.whiterose.ac.uk/id/eprint/147838/>

Version: Published Version

---

**Article:**

Castro, A.P.G., Altai, Z., Offiah, A.C. et al. (2019) Finite element modelling of the developing infant femur using paired CT and MRI scans. PLoS ONE, 14 (6). e0218268.  
ISSN: 1932-6203

<https://doi.org/10.1371/journal.pone.0218268>

---

**Reuse**

This article is distributed under the terms of the Creative Commons Attribution (CC BY) licence. This licence allows you to distribute, remix, tweak, and build upon the work, even commercially, as long as you credit the authors for the original work. More information and the full terms of the licence here:

<https://creativecommons.org/licenses/>

**Takedown**

If you consider content in White Rose Research Online to be in breach of UK law, please notify us by emailing [eprints@whiterose.ac.uk](mailto:eprints@whiterose.ac.uk) including the URL of the record and the reason for the withdrawal request.

## RESEARCH ARTICLE

## Finite element modelling of the developing infant femur using paired CT and MRI scans

A. P. G. Castro<sup>1,2</sup>, Z. Altai<sup>1</sup>, A. C. Offiah<sup>3</sup>, S. C. Shelmerdine<sup>4,5</sup>, O. J. Arthurs<sup>4,5</sup>, X. Li<sup>1\*</sup>, D. Lacroix<sup>1</sup>

**1** INSIGNEO Institute, Dept. of Mechanical Engineering, University of Sheffield, Sheffield, United Kingdom, **2** IDMEC, Instituto Superior Técnico, Universidade de Lisboa, Lisbon, Portugal, **3** Dept. of Oncology and Human Metabolism, University of Sheffield, Sheffield, United Kingdom, **4** Dept. of Radiology, Great Ormond Street Hospital for Children, London, United Kingdom, **5** UCL Great Ormond Street Institute for Child Health, University College London, London, United Kingdom

\* [xinshan.li@sheffield.ac.uk](mailto:xinshan.li@sheffield.ac.uk)

## Abstract

Bone finite element (FE) studies based on infant post-mortem computed tomography (CT) examinations are being developed to provide quantitative information to assist the differentiation between accidental and inflicted injury, and unsuspected underlying disease. As the growing skeleton contains non-ossified cartilaginous regions at the epiphyses, which are not well characterised on CT examinations, it is difficult to evaluate the mechanical behaviour of the developing whole bone. This study made use of paired paediatric post mortem femoral CT and magnetic resonance imaging (MRI) examinations at two different stages of development (4 and 7 months) to provide anatomical and constitutive information for both hard and soft tissues. The work aimed to evaluate the effect of epiphyseal ossification on the propensity to shaft fractures in infants. The outcomes suggest that the failure load of the femoral diaphysis in the models incorporating the non-ossified epiphysis is within the range of bone-only FE models. There may however be an effect on the metaphysis. Confirmation of these findings is required in a larger cohort of children.

## OPEN ACCESS

**Citation:** Castro APG, Altai Z, Offiah AC, Shelmerdine SC, Arthurs OJ, Li X, et al. (2019) Finite element modelling of the developing infant femur using paired CT and MRI scans. PLoS ONE 14(6): e0218268. <https://doi.org/10.1371/journal.pone.0218268>

**Editor:** Jose Manuel Garcia Aznar, University of Zaragoza, SPAIN

**Received:** January 18, 2019

**Accepted:** May 29, 2019

**Published:** June 18, 2019

**Copyright:** © 2019 Castro et al. This is an open access article distributed under the terms of the [Creative Commons Attribution License](https://creativecommons.org/licenses/by/4.0/), which permits unrestricted use, distribution, and reproduction in any medium, provided the original author and source are credited.

**Data Availability Statement:** The data underlying this article are not publicly available due to its sensitivity. Ethical approval and parental consent were obtained for the use of these post mortem paediatric and perinatal images for research purposes only. Working and supporting data (finalised computational models and/or simulation outputs) may be available upon agreement: please contact [xinshan.li@sheffield.ac.uk](mailto:xinshan.li@sheffield.ac.uk) or [pmo@insigneo.org](mailto:pmo@insigneo.org) if interested in working on the files.

## Introduction

Bone fractures in the United Kingdom account for 10–25% of accidental injuries in children [1]. Of these, long bones (e.g., femur, tibia or radius) have the highest fracture rates [2–4]. A survey conducted of 382 children aged 2–14 years old found that 41.6% of fractures occurred at home [5]. It has also been reported that 25% of injuries in children aged 12 months or younger are inflicted [6,7]. Most fractures seen in child abuse occur in children younger than 3 years old, with 80% occurring before 18 months [2,4]. The determination of whether the injuries are accidental or not depends largely on clinician's experience, as no reliable quantitative diagnostic tools are available [3,8,9]. Diagnosing child abuse continues to be a challenging task for experienced clinicians with potential negative consequences. Reports have shown that a significant number of infant child abuse cases are at first misdiagnosed (or missed) [2,10], which may lead to further harm [9,11,12]. Given this scenario, there is a need to clarify the

**Funding:** Funding from EPSRC ("Multisim", grant no. EP/K03877X/1) is acknowledged. A. P. G. Castro acknowledges funding from Portuguese Science and Technology Foundation through LAETA project UID/EMS/50022/2019 and PTDC/BBB-BMC/5655/2014. O. J. Arthurs is funded by an NIHR Clinician Scientist Fellowship. This article presents independent research funded by the National Institute for Health Research (NIHR) and supported by the Great Ormond Street Hospital Biomedical Research Centre. The views expressed are those of the authors and not necessarily those of the NHS, the NIHR or the Department of Health.

**Competing interests:** The authors have declared that no competing interests exist.

mechanisms of childhood injury, particularly in children yet to develop appropriate communication skills [4,6].

The growing skeleton contains non-ossified cartilaginous regions at the epiphyses (up to 35% non-ossified in infants [13]) and the femoral head only completely ossifies around 14 years of age [14,15]. Therefore the femoral head is not well characterised by computed tomography (CT) scans. In contrast, magnetic resonance imaging (MRI) shows cartilage more clearly, providing anatomical information for soft tissues, while avoiding exposure to radiation [15–18]. Although finite element (FE) models available in the literature are not fully representative of the complete age range of younger children, they already provide preliminary quantitative information to differentiate accidental from inflicted injury [19–22]. However, none of these models include geometric detail of the ossifying regions of the long bone. A combination of CT and MRI would therefore lead to the development of improved FE models of immature long bones (with more precise geometries).

Previous work on paired CT/MRI examinations include evaluation of the human temporal bone [23] and the porcine femur [24]. In the specific area of FE models generated from CT and MRI, the range of applications include the human adult tibiofemoral joint [25] and the intervertebral disc [26]. However, to the authors' best knowledge, co-registration of the two imaging modalities towards modelling of human infant bone has not been previously reported.

This work proposes a methodology to combine femoral CT and MRI examinations of the same child, exploiting the advances in commercially available imaging and modelling software. This new framework is intended to contribute to the development of more complete FE models of growing infant bones, incorporating the contribution of tissues at different levels of mineralisation [8,14,27,28]. An immediate application of this work is to elucidate the mechanisms of metaphyseal fractures [20], which is not well studied due to the lack of information or method to capture the ossifying region of the epiphysis. In the long term, such an approach is expected to enhance our understanding of the biomechanics of the developing femoral head [3,19,29,30] and differentiating accidental from inflicted injury.

## Methods

We used paired post-mortem CT and MRI scans of two infants (age 4 and 7 months), selected from the post mortem paediatric and perinatal imaging database of the Radiology Department, Great Ormond Street Hospital, London [31,32]. Cause of death was not disclosed. However, images were reviewed by experienced radiologists to ensure that the skeleton appeared normal on the scans. Ethical approval and parental consent were obtained for the use of these images for research purposes (LREC 13/LO/1494). At the time of the study, there were only two cases from this database having at least the proximal part of the femur clearly visible on both imaging modalities and aged under 18 months (4 and 7 months), and therefore still having a substantial portion of ossifying cartilage in the epiphysis.

The bony geometry of the femoral diaphysis was obtained from CT examinations and the cartilaginous tissues of the ossifying proximal femoral head region were obtained from MRI. The protocol consisted of independent segmentation of the CT and MRI data, using Amira 6.3 (FEI Visualization Sciences Group, France). CT segmentation was performed semi-automatically (through adjustable threshold), while MRI segmentation was manual. Using the multiplanar views tool available in Amira, the segmented regions of interest were matched and aligned. This alignment (and repositioning) was based on the manual alignment of the ossifying region with respect to the femoral diaphysis, using the epiphyseal area as the reference. Independent 3D surface models were then generated and imported into

ScanIP 7.0 (Simpleware Ltd, UK). This software allows for the combination of the independent surface models into a single surface model, resulting in the generation of a FE model that contains both the bony diaphysis and the cartilaginous proximal femoral head (Fig 1). This protocol ensures a continuous subject-specific geometry of the femur and can be readily applied to other developing long bones.

The 4-month-old model had 137493 nodes and 94922 elements, while the 7-month-old model had 161969 nodes and 111261 elements. Both models used 10-node tetrahedral elements. The material properties of each FE model were subject-specific (estimated from CT attenuation) and estimated using Bonemat V3 (Rizzoli Institute, Italy) [33]. This is in contrast to common material properties used in infant studies, which are usually scaled-down from adult data [14,34]. This software calculates an averaged Young's modulus for each element, integrated from surrounding pixels in the original CT scans [19,33,35]. The calibration methods and mathematical relationships applied were taken from Li et al. (2015), from which further information on image calibration and material property extraction from Bonemat is

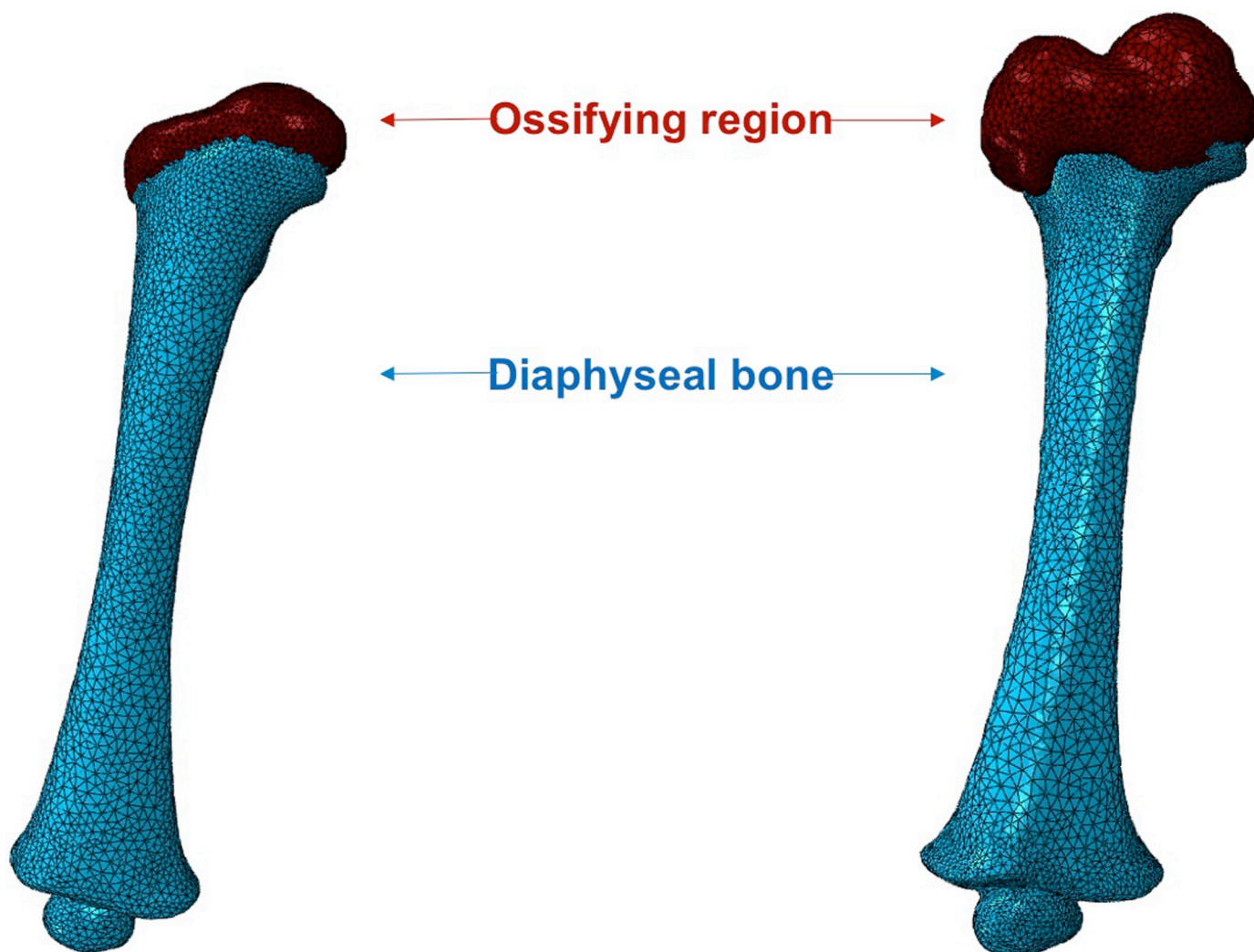


**Fig 1. FE models of infant femur (left– 4 months; right– 7 months).** Femoral dimensions are given in Table 1. Please note that only the proximal ossifying region was present in the MRI scans, i.e., the distal ossifying region was not extracted from the MRI scans.

<https://doi.org/10.1371/journal.pone.0218268.g001>

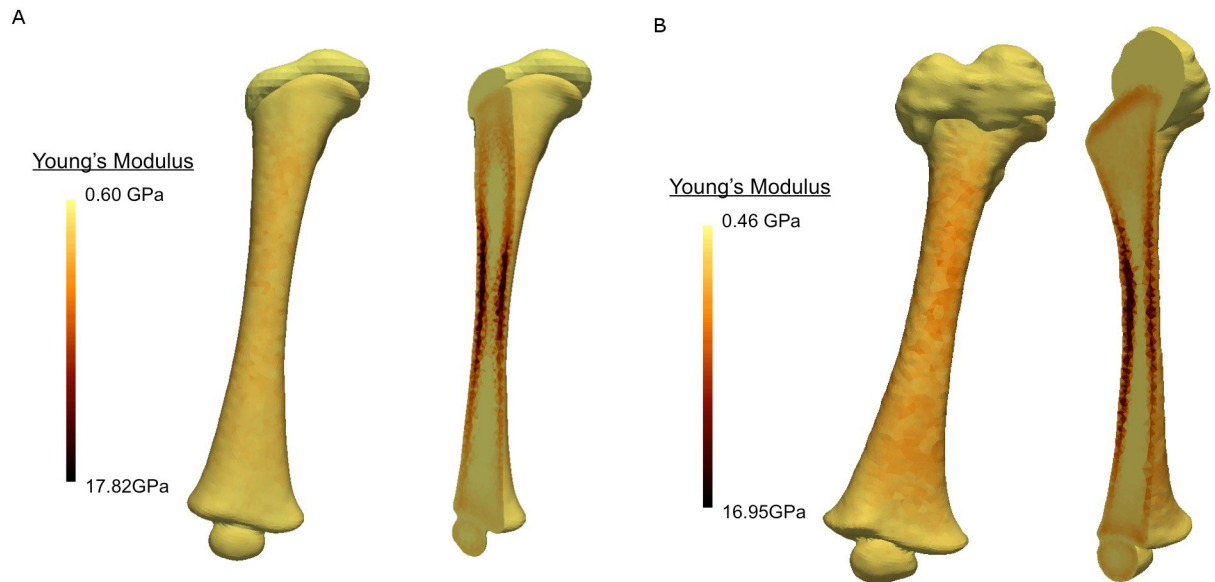


**Fig 2. Subject-specific material properties and distribution.** a) 4 months; b) 7 months. The maximum stiffness in the cortical bone is approximately 16–18 GPa for both models. The average Young’s modulus for the ossifying region is estimated to be between 0.46 and 0.60 GPa. The transition between ossifying and mineralised bone can be clearly seen towards the proximal and distal ends.

<https://doi.org/10.1371/journal.pone.0218268.g002>

available. The distribution of Young’s modulus along each model is shown in Fig 2, where a smooth transition between diaphyseal and ossifying regions can be seen. It must be highlighted that the properties of the ossifying region (i.e., the cartilaginous epiphysis) were also estimated from the CT scans (since this region could be considered transitional between cartilage and bone), in order to provide subject-specific material estimation for the porohyperelastic material (as described in the following paragraph).

Despite the significant difference in the size of each femur, the Young’s modulus range is similar (0.60–17.82 GPa for the 4 month old infant and 0.46–16.95 GPa for 7 the month old) and aligned with the known literature [36–38]. The cross-sectional epiphyseal area between the diaphysis and the ossifying region was calculated, as well as the volume of the proximal epiphyses: the 7 months epiphysis is about 6.4 times that of the 4-month old (see Table 1). The areas corresponding to the diaphysis were modelled as isotropic linear elastic (as per Bonemat’s attribution); a detailed description of the material model can be found in Li et al. (2015). The ossifying region was modelled as porohyperelastic (linear permeability and Neo Hookean solid model), following a widely used approach to model cartilaginous soft tissue. The Neo Hookean parameters ( $C_{10}$  and  $D_1$ , in Eq 1, which are associated with the stiffness of the material) were calculated [39] from the Young’s modulus value ( $E$ ) extracted from Bonemat, using Eqs 2 and 3, where  $\nu$  is the Poisson’s ratio, with a value of 0.20, taken from the literature

**Table 1. Dimensions of the infant femur FE models.**

|  | 4 months | 7 months |
|--|----------|----------|
| Proximal-distal length (cm)                        | 10.55    | 13.28    |
| Epiphyseal cross-sectional area (cm <sup>2</sup> ) | 2.14     | 3.37     |
| Proximal epiphysis volume (cm <sup>3</sup> )       | 1.24     | 7.91     |
| Total volume (cm <sup>3</sup> )                    | 13.13    | 30.79    |

<https://doi.org/10.1371/journal.pone.0218268.t001>

[20,40]. Poroelastic properties were also extracted from the literature [41]. A summary of the material properties is shown in Table 2.

$$\bar{W}_{NH}(C) = C_{10}(\bar{I}_1 - 3) + \frac{1}{D_1}(J - 1)^2 \tag{1}$$

$$C_{10} = \frac{E}{4(1 + \nu)} \tag{2}$$

$$D_1 = \frac{6(1 - 2\nu)}{E} \tag{3}$$

In order to obtain more accurate boundary conditions, previous work proposed a coordinate system for the femur where two cross-sections of the diaphysis were identified at 25% and 75% of its total length [22]. The same coordinate system was used in this study in order to compare current results with those of the previous publication. The centroids of these two cross-sections were estimated, and the X-axis was defined as a line passing through both centroids, running from proximal to distal. A positive Y-axis points medially and a positive Z-axis points to the anterior perpendicular to the X-Y plane. This coordinate system (Fig 3) ensures the minimisation of the implicit bending effect due to anatomical asymmetry of the femur [19,22]. The anatomical reference points (1 and 2) were also selected to be consistent with the bone only study by Li et al., 2015 [19], in which inter- and intra-observer reliability tests revealed these points to be the most reliable landmarks.

Two sets of experiments were carried out, namely torsion and uniaxial loading. Both loads were applied at Point 1, keeping the femur fixed for all degrees of freedom at Point 2. Torsion around the longitudinal axis was applied to mimic a twist to the femur, and the three uniaxial loads were chosen to represent direct impact load applied to the bone (at Point 1) in each of the X, Y, and Z directions. Point 1 was selected for application of the load because it is the ossification centre for the proximal femur, which will become the femoral head once fully mineralised. This is in line with the approach taken in studies of adult femurs.

For torsion, external moment of 2kN.mm was applied, in order to compare the moment to fail of these models (femur with bone plus ossifying region) with the analogous simulations performed by Altai et al. (2018) [22] in their model (femoral diaphysis only). The moment to fail corresponds to the maximum strains or the threshold of elastic strain limit, which were reported to be 0.73% in tension and 1.04% in compression, following the works of Bayraktar et al. (2004) [42] and Schileo et al. (2007) [43] on adult bone. It must be highlighted that only the diaphysis was considered for this calculation. For the uniaxial loads of 200N, different directions were selected to reveal which efforts would be more relevant to induce highly localised stress-strain levels on the infant femur and potentially lead to metaphyseal or shaft fractures. The FE simulations were performed with Abaqus 6.13 (Dassault Systèmes Simulia Corp., USA).

**Table 2. Material properties of the ossifying region (proximal epiphyses) for the two models.**

|  | 4 months | 7 months |
|--|----------|----------|
| Permeability (m <sup>4</sup> /Ns) [41] |          | 0.00455  |
| Void ratio [41]                        |          | 4.50     |
| Poisson's ratio [20,40]                |          | 0.20     |
| C <sub>10</sub> (MPa)                  | 125.34   | 96.09    |
| D <sub>1</sub>                         | 0.0060   | 0.0078   |

<https://doi.org/10.1371/journal.pone.0218268.t002>

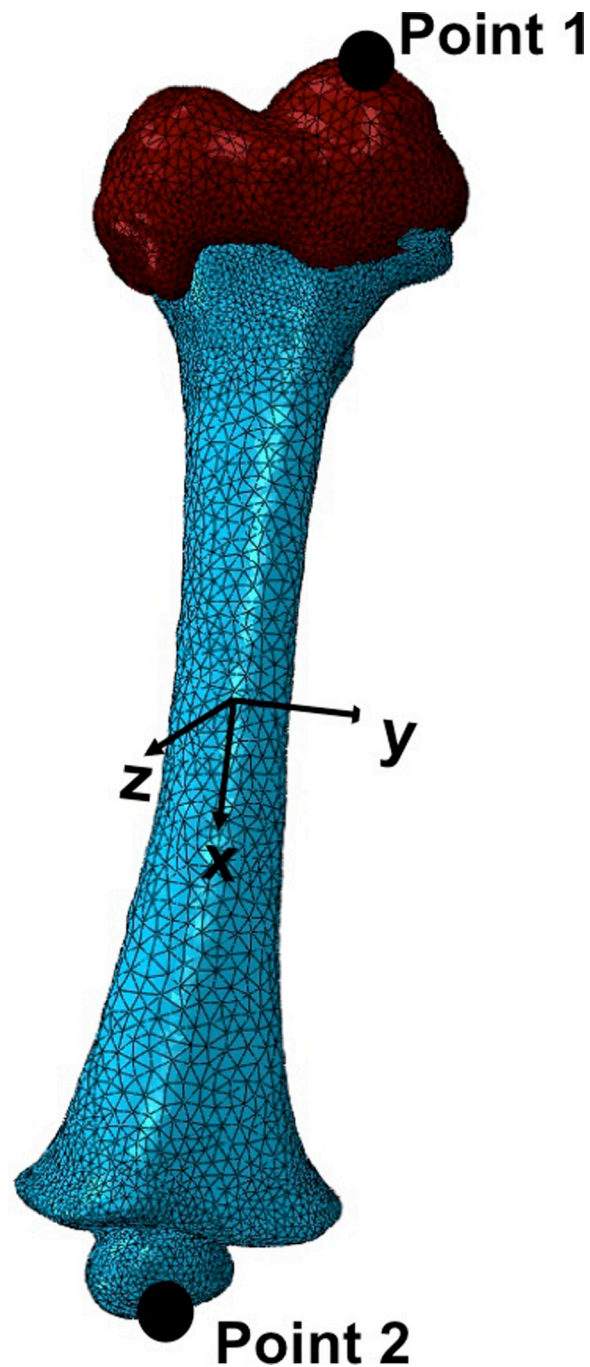


**Fig 3.** Coordinates system for the infant femur, with the reference points for applying the loading conditions.

<https://doi.org/10.1371/journal.pone.0218268.g003>

## Results

The maximum principal strain distributions in the two femur models under torsion are shown in Fig 4. The maximum principal strain range on the 4 months model was  $4.1 \times 10^{-06}$  to  $2.9 \times 10^{-01}$ , compared to  $9.0 \times 10^{-07}$  to  $5.3 \times 10^{-02}$  on the 7 months model. The area of high strain was located on the femoral diaphysis. The developing greater trochanter appeared to be almost strain-free, while some strain concentration appeared to build up around the epiphyses,

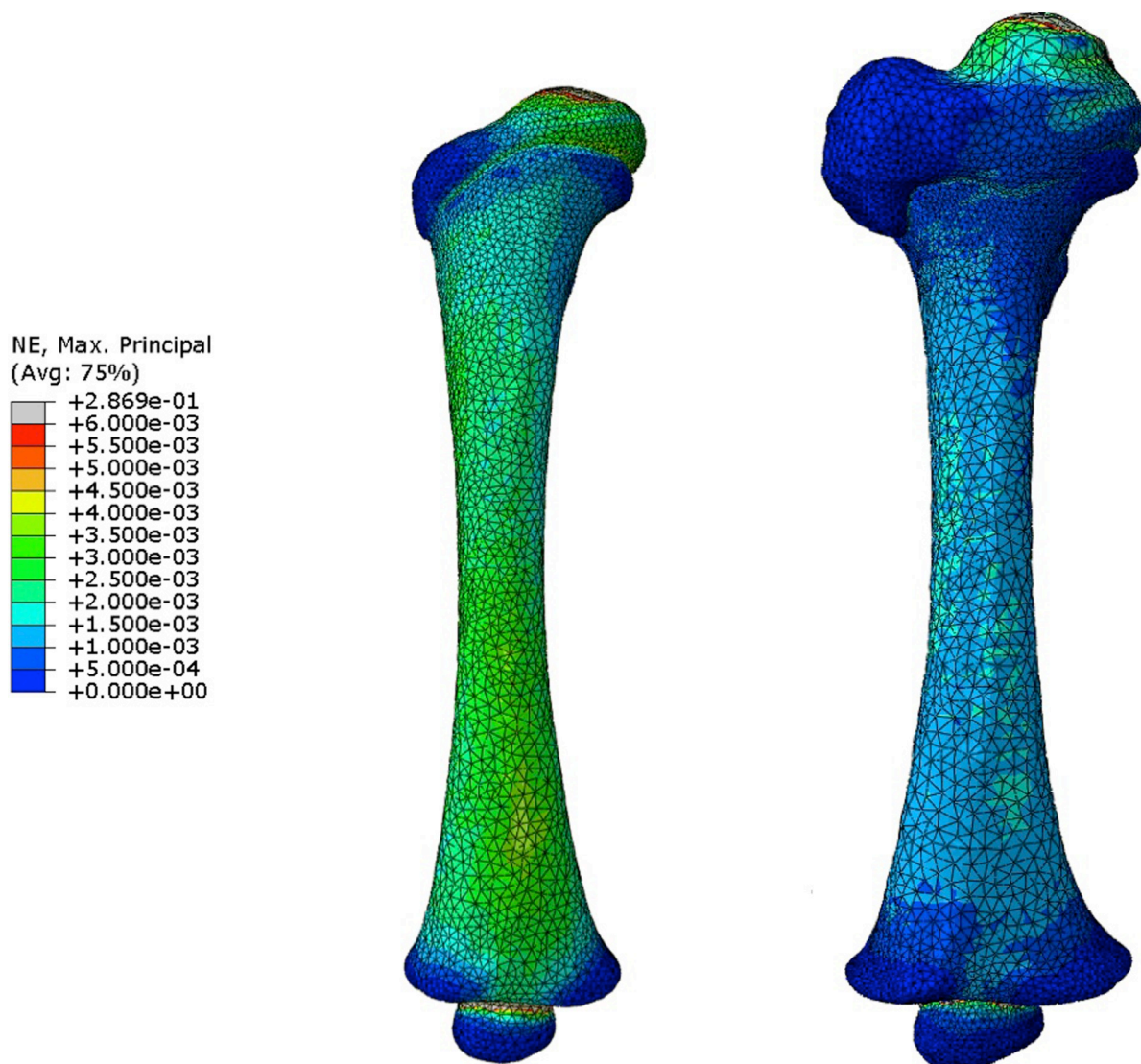


**Fig 4. Maximum principal strain distributions for a 2kN.mm external moment applied on infant femur (left- 4 months; right- 7 months).**

<https://doi.org/10.1371/journal.pone.0218268.g004>

particularly in the 4 months model. The moment to failure evaluated in these two models were compared against the values obtained from previous simulations performed exclusively on the femoral diaphysis [22], which yielded very similar results. The comparison of moment to fail calculations is shown in Fig 5.

The maximum principal strains under uniaxial loads predicted for the 4 months model are visibly higher than those of the 7 months model, as shown in Fig 6 (4-month-old) and Fig 7 (7-month-old), respectively. Maximum principal strains is plotted since the bone first failed in tension.

These uniaxial loads seem to be promoting strain accumulation on the diaphyseal regions, which means the epiphyses were less deformed. Femoral head deformation was most evident following the bending effect of the load applied on the Z-axis (anterior-posterior direction), regardless of developmental stage of the femur.

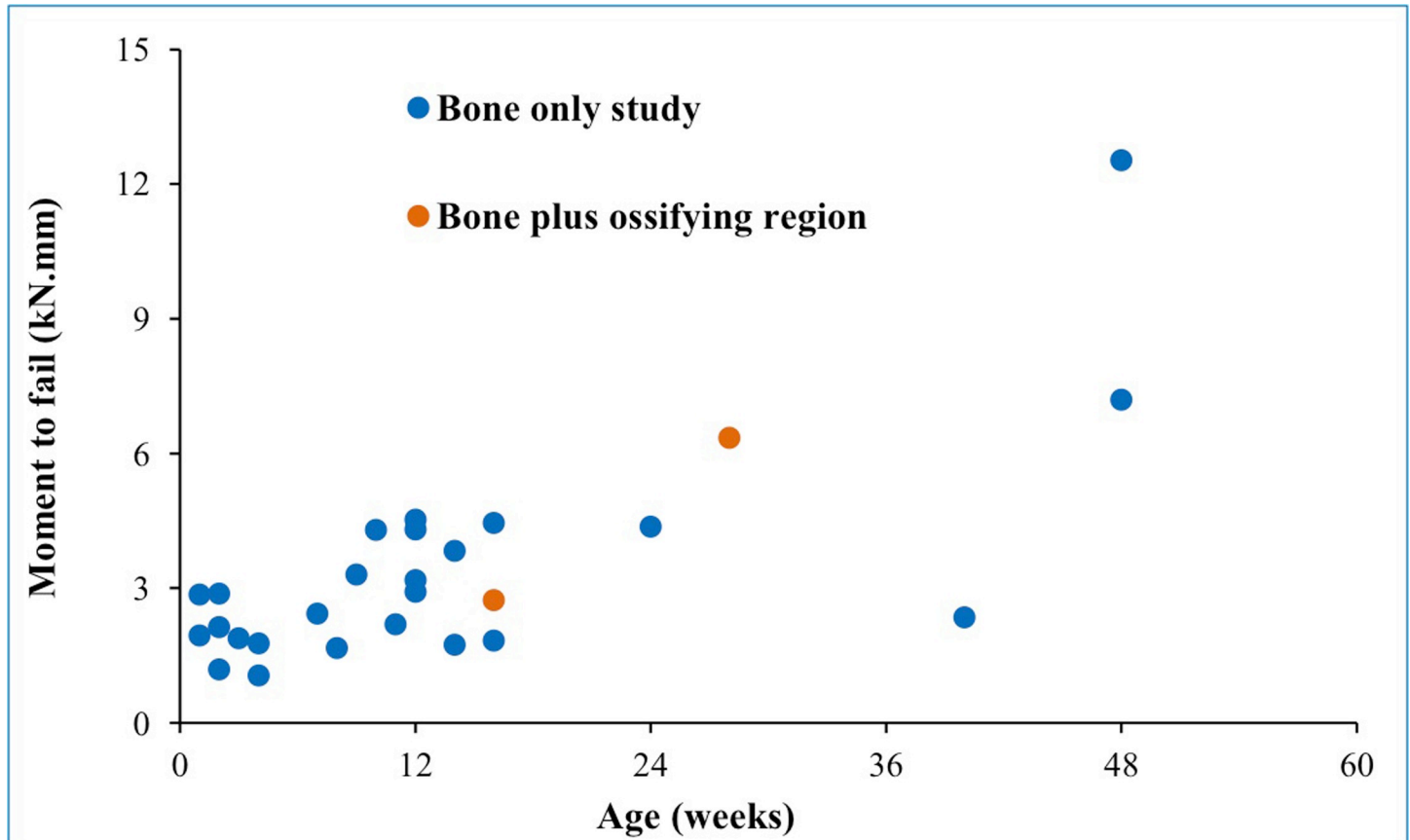


**Fig 5. Moment to fail of infant femurs, comparing bone only calculations from Altai et al. (2018) with current results for bone plus ossifying cartilaginous region.** Note that a different CT-only dataset was used in Altai et al. (2018).

<https://doi.org/10.1371/journal.pone.0218268.g005>

## Discussion

This study suggests that the proximal epiphysis is not as significant for the biomechanics of the whole infant femur as has previously been speculated [20,44,45]. The comparison with FE models of bone only infant femora models [22] showed an agreement with the moment to fail, for both the 4 and the 7 months old subjects.

Regarding the characterization of the proximal ossifying region, it was observed that the material transition from the diaphysis to the cartilage-based soft tissues is smooth, reflecting the mineralisation process. Although the method for calibration applied through Bonemat was originally developed for bony material on CT scans, the authors believe this is the best possible approach to obtain representative mechanical properties of that individual given the scarce data available to describe children's cartilage material properties. An alternative approach would be to assume adult articular or hyaline cartilage property for this region, which is likely to differ from infants. The thickness of the ossifying region is very different from regular cartilage layers, and the current knowledge of the mineralisation process of developing bone suggests that this region is formed of an intermediate material between bone and cartilage [8,18,27,29]. Plus, the material properties extracted from Bonemat (Young Modulus in the range of 460–600 MPa) indicate towards a transitional material between what is known for adult cartilage (Young Modulus in the range of 1–10MPa [46,47]) and bone. Another limitation of this study is that the bone was modelled as isotropic linear elastic. Although this is a

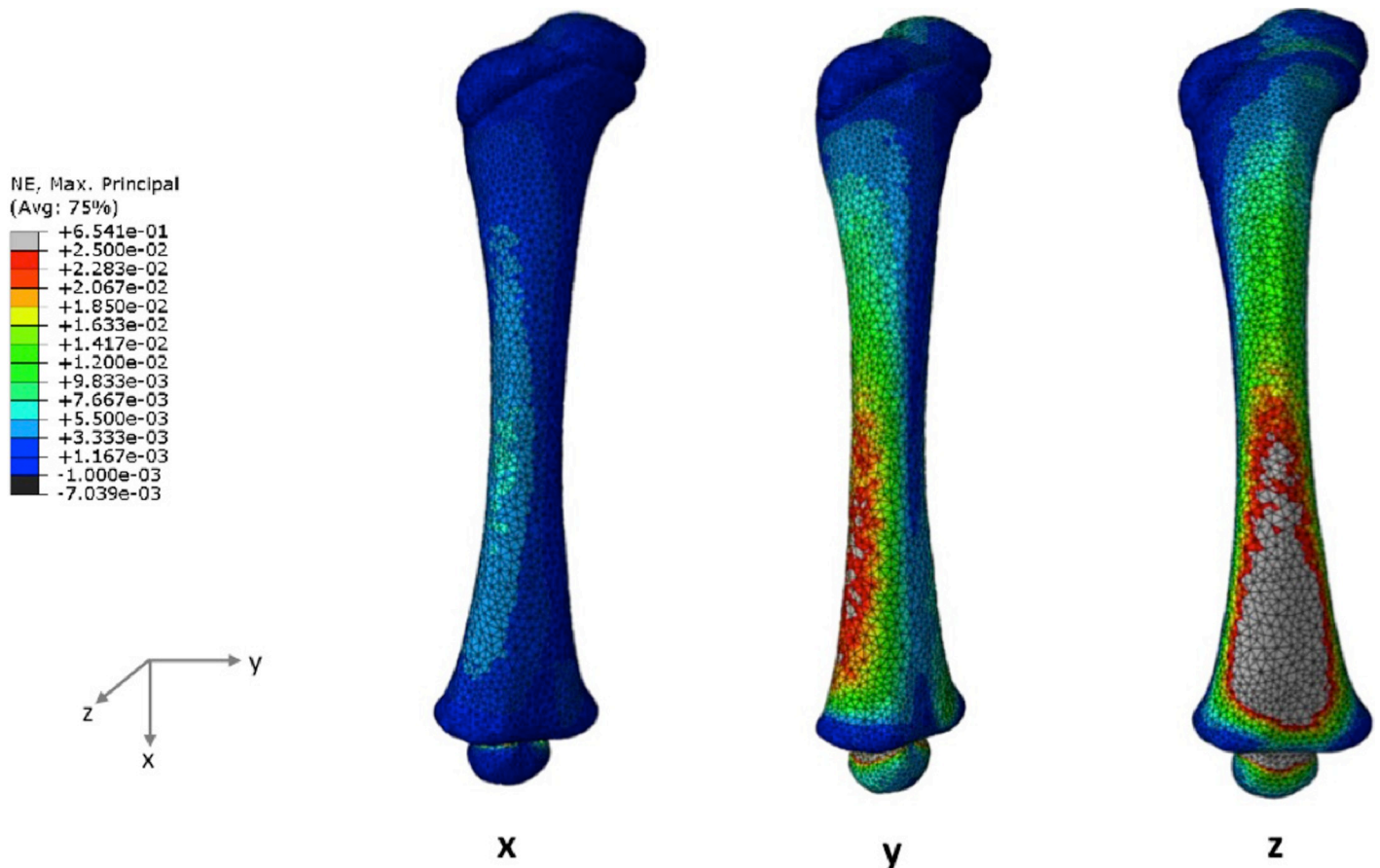


**Fig 6.** Maximum principal strain distributions when a uniaxial load is applied in the X-, Y- or Z-axis for the 4 months model.

<https://doi.org/10.1371/journal.pone.0218268.g006>

common simplification, the effect of anisotropy on the whole bone (including ossifying region) needs to be addressed in the future.

Pure uniaxial compression through the proximal-distal length of the femur could not be achieved due to asymmetry of the femur. These loading conditions resulted in a combination of lateral compression and bending. As such, the effect of the direct load (200N) was reduced, particularly when compared with the bending caused by the other two uniaxial loading conditions (Y- and Z-axes in this coordinate system). These conditions help to extrapolate how the infant femur responds to potentially harmful pushing or pulling movements in different directions. Given that the major deformation occurred with frontal bending loads (Z-axis) and that this movement is likely to be clinically associated with inflicted injury, one can speculate that frontal plane infant femoral injuries/fractures have greater probability of being associated with physical abuse through excessive loading than torsion or other uniaxial loads [7,29,45]. It should be also noted that although the loading conditions applied here were simplified, as in other work on developing bones (e.g., Tsai et al. 2017), they were related to the magnitude and direction of abuse-inflicted injuries. Typically, a combination of these loads would occur in a real-world infant injury scenario, such as those causing the classic metaphyseal lesion [48]. To the authors' best knowledge, there has been only one previous modelling paper on the classic metaphyseal lesion [20], in which the authors excluded the epiphysis, making the assumption that "any influence of the physis or ligaments on the relative strain patterns would be negligible". However, the current study does indicate that the strain distribution changes within the

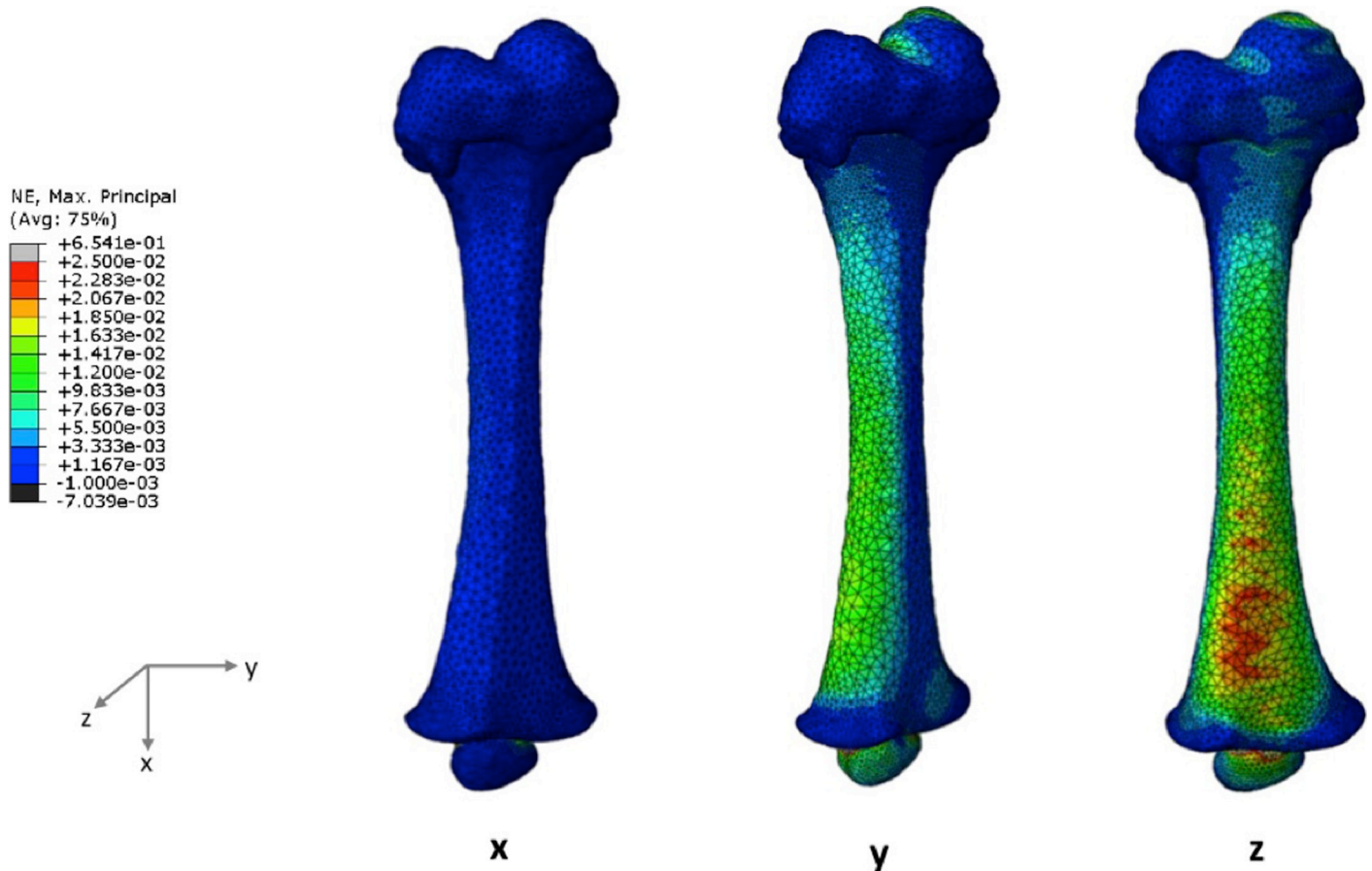


**Fig 7. Maximum principal strain distributions when a uniaxial load is applied in the X-, Y- or Z-axis for the 7 months model.**

<https://doi.org/10.1371/journal.pone.0218268.g007>

transition region and this is worth further investigation. The biggest impacts of including the epiphysis seems to be twofold: (a) there is now an area of concentrated strain at the transition region; and (b) the epiphysis itself suffers from highly localised strain, even though the overall mechanical behaviour of the shaft is largely unaffected. Our results indicate that injuries close to the epiphysis should be modelled with caution, since the mineralising cartilaginous epiphysis does seem to have an effect on local strain distribution.

There is very limited paired CT/MRI imaging data available containing both the femoral diaphysis and proximal femoral head, contributing to the lack of previous studies on the non-ossified regions of the long bones, but the two subjects in this current study show proof of principle in the target population. This would provide a new and non-invasive image-based approach to investigate young children's bone properties, complementing previous mechanical studies of cadaveric bone samples, which are also scarce [10,36–38]. The developed approach could also be useful to validate failure predictions on paired CT-MRI FE models of young animal bones, by comparing with destructive results. Future work should include more infant cases considering a wider range of developmental stages, up to 3 years old [4]. The establishment of well-defined landmarks or accurate measurement and marking of the epiphyseal area may improve the accuracy of the process, although manual adjustments might still be needed to ensure consistent representation of the femoral anatomy.

In conclusion, this work introduces a new approach to incorporate both bone and ossifying cartilage in FE models of the infant femur, on both geometrical and constitutive aspects of modelling. The results suggest that the proximal ossifying region has no significant effect on the moment to fail of the infant femoral shaft under torsion, although axial loading in the proximal femur produced variable results around the metaphyseal region that require further investigation.

## Acknowledgments

Funding from EPSRC (“Multisim”, grant no. EP/K03877X/1) is acknowledged.

A. P. G. Castro acknowledges funding from Portuguese Science and Technology Foundation through LAETA project UID/EMS/50022/2019 and PTDC/BBB-BMC/5655/2014.

O. J. Arthurs is funded by an NIHR Clinician Scientist Fellowship. This article presents independent research funded by the National Institute for Health Research (NIHR) and supported by the Great Ormond Street Hospital Biomedical Research Centre. The views expressed are those of the author(s) and not necessarily those of the NHS, the NIHR or the Department of Health.

## Author Contributions

**Conceptualization:** A. P. G. Castro.

**Data curation:** A. P. G. Castro, X. Li.

**Funding acquisition:** D. Lacroix.

**Investigation:** A. P. G. Castro, Z. Altai, S. C. Shelmerdine.

**Methodology:** A. P. G. Castro, Z. Altai, S. C. Shelmerdine, O. J. Arthurs.

**Project administration:** D. Lacroix.

**Supervision:** A. C. Offiah, O. J. Arthurs, X. Li, D. Lacroix.

**Validation:** X. Li.

**Writing – original draft:** A. P. G. Castro.

**Writing – review & editing:** A. P. G. Castro, Z. Altai, A. C. Offiah, S. C. Shelmerdine, O. J. Arthurs, X. Li, D. Lacroix.

## References

1. Cooper C, Dennison EM, Leufkens HG, Bishop N, van Staa TP. Epidemiology of Childhood Fractures in Britain: A Study Using the General Practice Research Database. *J Bone Miner Res*. 2004; 19: 1976–1981. <https://doi.org/10.1359/JBMR.040902> PMID: 15537440
2. Ravichandiran N, Schuh S, Bejuk M, Al-Harthy N, Shouldice M, Au H, et al. Delayed Identification of Pediatric Abuse-Related Fractures. *Pediatrics*. 2010; 125: 60–66. <https://doi.org/10.1542/peds.2008-3794> PMID: 19948569
3. Lonergan GJ, Baker AM, Morey MK, Boos SC. From the Archives of the AFIP. *RadioGraphics*. 2003; 23: 811–845. <https://doi.org/10.1148/rg.234035030> PMID: 12853657
4. Brown D, Fisher E. Femur Fractures in Infants and Young Children. *Am J Public Health*. 2004; 94: 558–560. <https://doi.org/10.2105/ajph.94.4.558> PMID: 15054003
5. Valerio G, Gallè F, Mancusi C, Di Onofrio V, Colapietro M, Guida P, et al. Pattern of fractures across pediatric age groups: analysis of individual and lifestyle factors. *BMC Public Health*. BioMed Central Ltd; 2010; 10: 656. <https://doi.org/10.1186/1471-2458-10-656> PMID: 21034509
6. Baker R, Orton E, Tata LJ, Kendrick D. Risk factors for long-bone fractures in children up to 5 years of age: a nested case-control study. *Arch Dis Child*. 2015; 100: 432–7. <https://doi.org/10.1136/archdischild-2013-305715> PMID: 25398446

7. Barber MA, Sibert JR. Diagnosing physical child abuse: the way forward. *Postgrad Med J*. 2000; 76: 743–9. <https://doi.org/10.1136/pmj.76.902.743> PMID: 11085763
8. Gallo S, Vanstone CA, Weiler HA. Normative data for bone mass in healthy term infants from birth to 1 year of age. *J Osteoporos*. 2012; 2012: 672403. <https://doi.org/10.1155/2012/672403> PMID: 23091773
9. Jenny C. Evaluating Infants and Young Children With Multiple Fractures. *Pediatrics*. 2006; 118: 1299–1303. <https://doi.org/10.1542/peds.2006-1795> PMID: 16951031
10. Prosser I, Lawson Z, Evans A, Harrison S, Morris S, Maguire S, et al. A timetable for the radiologic features of fracture healing in young children. *Am J Roentgenol*. 2012; 198: 1014–1020. <https://doi.org/10.2214/AJR.11.6734> PMID: 22528890
11. Hindley N. Risk factors for recurrence of maltreatment: a systematic review. *Arch Dis Child*. 2006; 91: 744–752. <https://doi.org/10.1136/adc.2005.085639> PMID: 16840503
12. Pandya NK, Baldwin K, Kamath AF, Wenger DR, Hosalkar HS. Unexplained fractures: Child abuse or bone disease. A systematic review. *Clin Orthop Relat Res*. 2011; 469: 805–812. <https://doi.org/10.1007/s11999-010-1578-z> PMID: 20878560
13. Scheuer L, Black S, Christie A. *Developmental Juvenile Osteology*. Elsevier Inc; 2000.
14. Forestier-Zhang L, Bishop N. Bone strength in children: understanding basic bone biomechanics. *Arch Dis Child Educ Pract Ed*. 2016; 101: 2–7. <https://doi.org/10.1136/archdischild-2015-308597> PMID: 26269494
15. Pinheiro M, Dobson CA, Perry DC, Fagan MJ. New insights into the biomechanics of Legg-Calvé-Perthes' disease: The role of epiphyseal skeletal immaturity in vascular obstruction. *Bone Joint Res*. 2018; 7. <https://doi.org/10.1302/2046-3758.73.BJR-2017-0191.R1>
16. Farr JN, Amin S, Melton LJ, Kirmani S, McCready LK, Atkinson EJ, et al. Bone Strength and Structural Deficits in Children and Adolescents With a Distal Forearm Fracture Resulting From Mild Trauma. *J Bone Miner Res*. 2014; 29: 590–599. <https://doi.org/10.1002/jbmr.2071> PMID: 23959563
17. Zhu Y, Bermond F, Payen de la Garanderie J, Pialat J-B, Sandoz B, Brizard D, et al. In Vivo Assessment of Elasticity of Child Rib Cortical Bone Using Quantitative Computed Tomography. *Appl Bionics Biomech*. 2017; 2017: 1–9. <https://doi.org/10.1155/2017/2471368> PMID: 28835733
18. Bachrach LK. Bone mineralization in childhood and adolescence. *Curr Opin Pediatr*. 1993; 5: 467–73. PMID: 8374675
19. Li X, Viceconti M, Cohen MC, Reilly GC, Carre MJ, Offiah AC. Developing CT based computational models of pediatric femurs. *J Biomech*. 2015; 48: 2034–2040. <https://doi.org/10.1016/j.jbiomech.2015.03.027> PMID: 25895643
20. Tsai A, Coats B, Kleinman PK. Biomechanics of the classic metaphyseal lesion: finite element analysis. *Pediatr Radiol. Pediatric Radiology*; 2017; <https://doi.org/10.1007/s00247-017-3921-y> PMID: 28721473
21. Tsai A, Coats B, Kleinman PK. Stress profile of infant rib in the setting of child abuse: A finite element parametric study. *J Biomech. Elsevier*; 2012; 45: 1861–1868. <https://doi.org/10.1016/j.jbiomech.2012.05.049> PMID: 22727522
22. Altai Z, Viceconti M, Offiah AC, Li X. Investigating the mechanical response of paediatric bone under bending and torsion using finite element analysis. *Biomech Model Mechanobiol*. 2018; 17: 1001–1009. <https://doi.org/10.1007/s10237-018-1008-9> PMID: 29525976
23. Bartling SH, Peldschus K, Rodt T, Kral F, Matthies H, Kikinis R, et al. Registration and fusion of CT and MRI of the temporal bone. *J Comput Assist Tomogr*. 2005; 29: 305–310. <https://doi.org/10.1097/O1.rct.0000160425.63884.5b> PMID: 15891495
24. Lee YS, Seon JK, Shin VI, Kim G-H, Jeon M. Anatomical evaluation of CT-MRI combined femoral model. *Biomed Eng Online*. 2008; 7: 6. <https://doi.org/10.1186/1475-925X-7-6> PMID: 18234068
25. Carey RE, Zheng L, Aiyangar AK, Harner CD, Zhang X. Subject-Specific Finite Element Modeling of the Tibiofemoral Joint Based on CT, Magnetic Resonance Imaging and Dynamic Stereo-Radiography Data in Vivo. *J Biomech*. 2014; 136: 41004. <https://doi.org/10.1115/1.4026228> PMID: 24337180
26. Li H, Wang Z. Intervertebral disc biomechanical analysis using the finite element modeling based on medical images. *Comput Med Imaging Graph*. 2006; 30: 363–370. <https://doi.org/10.1016/j.compmedimag.2006.09.004> PMID: 17074465
27. Villemure I, Stokes IAF. Growth plate mechanics and mechanobiology. A survey of present understanding. *J Biomech*. 2009; 42: 1793–1803. <https://doi.org/10.1016/j.jbiomech.2009.05.021> PMID: 19540500
28. Cheong VS, Karunaratne A, Amis AA, Bull AMJ. Strain rate dependency of fractures of immature bone. *J Mech Behav Biomed Mater. Elsevier*; 2017; 66: 68–76. <https://doi.org/10.1016/j.jmbbm.2016.10.023> PMID: 27838592
29. Bishop N, Sprigg A, Dalton A. Unexplained fractures in infancy: looking for fragile bones. *Arch Dis Child*. 2007; 92: 251–256. <https://doi.org/10.1136/adc.2006.106120> PMID: 17337685

30. Albert C, Jameson J, Smith P, Harris G. Reduced diaphyseal strength associated with high intracortical vascular porosity within long bones of children with osteogenesis imperfecta. *Bone*. Elsevier Inc.; 2014; 66: 121–130. <https://doi.org/10.1016/j.bone.2014.05.022> PMID: 24928496
31. Arthurs OJ, van Rijn RR, Taylor AM, Sebire NJ. Paediatric and perinatal postmortem imaging: the need for a subspecialty approach. *Pediatr Radiol*. 2015; 45: 483–490. <https://doi.org/10.1007/s00247-014-3132-8> PMID: 25172007
32. Arthurs OJ, Taylor AM, Sebire NJ. Indications, advantages and limitations of perinatal postmortem imaging in clinical practice. *Pediatr Radiol*. 2015; 45: 491–500. <https://doi.org/10.1007/s00247-014-3165-z> PMID: 25274468
33. Schileo E, Dall'Ara E, Taddei F, Malandrino A, Schotkamp T, Baleani M, et al. An accurate estimation of bone density improves the accuracy of subject-specific finite element models. *J Biomech*. 2008; 41: 2483–2491. <https://doi.org/10.1016/j.jbiomech.2008.05.017> PMID: 18606417
34. Mizuno K, Iwata K, Deguchi T, Ikami T, Kubota M. Development of a Three-Year-Old Child FE Model. *Traffic Inj Prev*. 2005; 6: 361–371. <https://doi.org/10.1080/15389580500255922> PMID: 16266945
35. Taddei F, Pancanti A, Viceconti M. An improved method for the automatic mapping of computed tomography numbers onto finite element models. *Med Eng Phys*. 2004; 26: 61–69. [https://doi.org/10.1016/S1350-4533\(03\)00138-3](https://doi.org/10.1016/S1350-4533(03)00138-3) PMID: 14644599
36. Berteau JP, Baron C, Pithioux M, Launay F, Chabrand P, Lasaygues P. In vitro ultrasonic and mechanic characterization of the modulus of elasticity of children cortical bone. *Ultrasonics*. Elsevier B.V.; 2014; 54: 1270–1276. <https://doi.org/10.1016/j.ultras.2013.09.014> PMID: 24112598
37. Ambrose CG, Soto Martinez M, Bi X, Deaver J, Kuzawa C, Schwartz L, et al. Mechanical properties of infant bone. *Bone*. Elsevier; 2018; 113: 151–160. <https://doi.org/10.1016/j.bone.2018.05.015> PMID: 29800692
38. Meng Y, Untaroiu CD. A Review of Pediatric Lower Extremity Data for Pedestrian Numerical Modeling: Injury Epidemiology, Anatomy, Anthropometry, Structural, and Mechanical Properties. *Appl Bionics Biomech*. 2018; 2018: 1–19. <https://doi.org/10.1155/2018/6271898> PMID: 30254693
39. Iivarinen JT, Korhonen RK, Julkunen P, Jurvelin JS. Experimental and computational analysis of soft tissue mechanical response under negative pressure in forearm. *Ski Res Technol*. 2013; 19: 356–365. <https://doi.org/10.1111/j.1600-0846.2012.00652.x> PMID: 22650760
40. Lai YS, Chen WC, Huang CH, Cheng CK, Chan KK, Chang TK. The effect of graft strength on knee laxity and graft in-situ forces after posterior cruciate ligament reconstruction. *PLoS One*. 2015; 10: 1–11. <https://doi.org/10.1371/journal.pone.0127293> PMID: 26001045
41. Stender ME, Regueiro RA, Ferguson VL. A poroelastic finite element model of the bone-cartilage unit to determine the effects of changes in permeability with osteoarthritis. *Comput Methods Biomech Biomed Engin*. Taylor & Francis; 2016; 5842: 1–13. <https://doi.org/10.1080/10255842.2016.1233326> PMID: 27635796
42. Bayraktar HH, Morgan EF, Niebur GL, Morris GE, Wong EK, Keaveny TM. Comparison of the elastic and yield properties of human femoral trabecular and cortical bone tissue. *J Biomech*. 2004; 37: 27–35. [https://doi.org/10.1016/S0021-9290\(03\)00257-4](https://doi.org/10.1016/S0021-9290(03)00257-4) PMID: 14672565
43. Schileo E, Taddei F, Malandrino A, Cristofolini L, Viceconti M. Subject-specific finite element models can accurately predict strain levels in long bones. *J Biomech*. 2007; 40: 2982–2989. <https://doi.org/10.1016/j.jbiomech.2007.02.010> PMID: 17434172
44. Jaimes C, Chauvin N a, Delgado J, Jaramillo D. MR Imaging of Normal Epiphyseal Development and Common Epiphyseal Disorders. *Radiographics*. 2014; 34: 449–71. <https://doi.org/10.1148/rg.342135070> PMID: 24617691
45. Flaherty EG, Perez-Rossello JM, Levine MA, Hennrikus WL. Evaluating Children With Fractures for Child Physical Abuse. *Pediatrics*. 2014; 133: e477–e489. <https://doi.org/10.1542/peds.2013-3793> PMID: 24470642
46. Sánchez Egea AJ, Valera M, Parraga Quiroga JM, Proubasta I, Noailly J, Lacroix D. Impact of hip anatomical variations on the cartilage stress: A finite element analysis towards the biomechanical exploration of the factors that may explain primary hip arthritis in morphologically normal subjects. *Clin Biomech*. Elsevier Ltd; 2014; 29: 444–450. <https://doi.org/10.1016/j.clinbiomech.2014.01.004> PMID: 24530154
47. Pierce DM, Ricken T, Holzapfel G a. A hyperelastic biphasic fibre-reinforced model of articular cartilage considering distributed collagen fibre orientations: continuum basis, computational aspects and applications. *Computer Methods in Biomechanics and Biomedical Engineering*. Taylor & Francis; 2012. pp. 1–18. <https://doi.org/10.1080/10255842.2012.670854> PMID: 22764882
48. Forman JL, Dios P De, Symeonidis I, Duart J, Kerrigan JR, Salzar RS, et al. Fracture Tolerance Related to Skeletal Development and Aging Throughout Life: 3-Point Bending of Human Femurs. *IRCOBI Conf*. 2012; 524–539. <https://doi.org/10.1002/mrm.10658> PMID: 14705047